Electrocatalysis (2014) 5:125–135
DOI 10.1007/s12678-013-0173-y

Accelerated Stress Tests of Pt/HSAC Electrocatalysts: an Identical-Location Transmission Electron Microscopy Study on the Influence of Intermediate Characterizations

L. Castanheira · L. Dubau · F. Maillard

Published online: 22 November 2013

Abstract The influence of intermediate characterizations used in long-term accelerated stress tests (ASTs) to monitor the changes of the electrochemically active surface area of carbon-supported Pt nanoparticles (Pt/HSAC) was investigated. Our results indicate that, in the studied experimental protocol (potentiostatic polarization at $E = 1.0$ V vs. RHE during 96 h), the loss of the electrochemically active surface area is greatly exacerbated by intermediate characterizations such as cyclic voltammetry or stripping of a saturated CO_{ad} surface layer. These results can be understood in view of the breakdown of the passivation layer formed on the Pt/HSAC electrocatalyst during the polarization at $E = 1.0$ V vs. RHE. By using identical location transmission electron microscopy, the structural modifications of the Pt/HSAC nanoparticles could be monitored. The migration/agglomeration of Pt nanocrystallites, the growth of Pt nanocrystallites by electrochemical Ostwald ripening, and the corrosion of the high surface area carbon support are more pronounced when cyclic or CO_{ad} stripping voltammograms are implemented in the AST. A detailed analysis of the identical-location transmission electron microscopy images also indicates that adsorbed CO molecules minor the dissolution of Pt^{z+} ions into the electrolyte.

Keywords Proton exchange membrane fuel cells · Carbon-supported Pt nanoparticles · Electrocatalysts degradation mechanisms · Identical-location transmission electron microscopy · Intermediate characterizations

Electronic supplementary material The online version of this article (doi:10.1007/s12678-013-0173-y) contains supplementary material, which is available to authorized users.

L. Castanheira · L. Dubau · F. Maillard (✉)
Laboratoire d'Electrochimie et de Physico-chimie des Matériaux et des Interfaces, UMR 5279 CNRS/Grenoble INP/Université de Savoie/Université Joseph Fourier, 1130 rue de la piscine, BP 75, 38402 Saint Martin d'Hères Cedex, France
e-mail: frederic.maillard@lepmi.grenoble-inp.fr

Introduction

Proton exchange membrane fuel cells (PEMFCs) convert chemical energy of a fuel into clean electrical energy and represent a possible solution to diversify our energy portfolio. Over the past years, the research in PEMFC electrodes has focused in finding new cathode electrocatalysts that improve the rate of the sluggish cathodic oxygen reduction while maintaining the electrocatalyst's cost at a reasonable level [1–3]. Common cathode electrocatalysts are high surface area carbon-supported Pt (Pt/HSAC) or bimetallic Pt nanoalloys (Pt-alloy/HSAC) [4–9], but they undergo coarsening over time, therefore yielding a loss in electrochemical active surface area (ECSA). The degradation mechanisms of the carbon-supported Pt-based nanoparticles are now well identified: they involve the migration/agglomeration [9–12], the dissolution/redeposition (electrochemical Ostwald ripening) [13, 14], the corrosion of the carbon support, and the detachment of the metal nanoparticles [15–21].

Accelerated stress tests (ASTs) are commonly employed to study the performance and the robustness of different electrocatalysts and to avoid lengthy real-life PEMFC tests. Different organizations such as the American Department of Energy (DOE) and the Fuel Cell Commercialization Conference of Japan (FCCJ) have their own AST protocols [22, 23]. In the "Electrocatalyst Cycle and Metrics" test from the American DOE, a 30,000 triangle sweep cycle between 0.6 and 1.0 V vs. RHE is used. A polarization curve is performed each 1,000/5,000/10,000/30,000 cycles and cyclic voltammograms (CVs) are recorded every 10/100/1,000/3,000/10,000/20,000/30,000 cycles to monitor changes in ECSA and activity. In the "Catalyst Support Cycle and Metrics" test, which consists in a potentiostatic hold at 1.2 V for 400 h in a 25–50 cm^2 single cell, a polarization curve and a cyclic voltammetry are performed every 24 h. The Japanese FCCJ mimics start/stop cycles by a triangular wave potential

cycle between 1.0 and 1.5 V vs. RHE, and load cycles by a rectangular wave potential cycle between 0.6 and 1.0 V vs. RHE. Here again, CVs and polarization curves are recorded every 10 to 1,000 cycles. Such intermediate characterizations are considered to contribute only a minor part of the ECSA variations. However, since degradation processes are sensitive to the potential modulation mode (potential cycling vs. potential holding) [24, 25] and the investigated potential range [19, 25], the ECSA variations must be influenced or even emphasized by these intermediate characterization. Despite their great importance, the contribution of the intermediate characterization has not been discussed previously in the literature and is the focus of the present study.

This paper is aimed at investigating different methods of characterization (cyclic or CO_{ads} stripping voltammograms) to monitor changes in the ECSA of a Pt/HSAC electrocatalyst following a 96-h polarization at $E=1.0$ V vs. RHE and $T=330$ K. Identical-location transmission electron microscopy (IL-TEM) was employed to characterize the structure of the fresh/aged electrocatalysts. The results indicate that the degradation mechanism, and hence, the final value of ECSA strongly depend on the type and the number of intermediate characterizations.

Experimental

Electrocatalyst

The electrocatalyst used in this study is based on Pt nanoparticles supported on a high surface area carbon (HSAC). Such electrocatalyst was supplied by Tanaka Kikinzoku (TKK) and has a weight fraction (weight percent) of 40 % (TEC10E40E). The carbon support features a high surface area (800 $m^2\ g^{-1}$), and the surface-averaged Pt particle size is 2.3 nm. The electrocatalyst was used as-received without any further treatment.

Electrochemical Measurements

Solutions

The solutions were daily prepared from ultrapure water (MQ grade, 18.2 MΩ cm, 1–3 ppm TOC) and H_2SO_4 (Suprapur, Merck). The electrolyte was a 0.1 M H_2SO_4 solution purged with argon (Ar, >99.99 %, Messer).

Electrochemical Cell Setup

All the glassware used in this study was first cleaned by immersion in a H_2SO_4–H_2O_2 mixture overnight and thoroughly rinsed with MQ-grade water. The electrochemical characterization of the 40 wt.% Pt/HSAC electrocatalyst and the potentiostatic tests were conducted in two separated four-electrode electrochemical cells, a characterization and a degradation cell, both thermostated at $T=330$ K. A homemade rotating disk electrode (RDE) tip or an IL-TEM grid were used as working electrode and aged in two separated experiments. The counter-electrode was a Pt foil and the reference electrode—a mercury sulfate electrode (MSE) $Hg|Hg_2SO_4|K_2SO_4$ (saturated, aqueous)—connected to the cell via a Luggin capillary. This reference electrode was calibrated periodically by measuring the potential difference with a reversible hydrogen electrode (RHE), the latter being systematically 0.72 V. All the potentials reported in this study were referenced to that of the reversible hydrogen electrode (RHE). A Pt wire connected to the reference electrode was used to filter the high-frequency electrical noise and to avoid disturbing the low-frequency electrical measurements. More details on the dual-reference system used in this work can be found in Ref. [26].

Preparation of the Catalytic Layers

A suspension with a concentration of 0.735 $g_{Pt/C}L^{-1}$ of Pt/C composed of 5 wt.% Nafion® solution (Aldrich), MQ-grade water, and 40 wt.% Pt/HSAC was ultrasonically treated for 15 min to obtain a well-dispersed ink. Before each degradation test, the ink was ultrasonically treated for 6 min. Two additions of a 20-μl aliquot of this ink were loaded onto a home-made RDE made of glassy carbon (Sigradur, 0.196 cm^2) and Teflon® resulting in Pt loading of 60 $\mu g_{Pt}\ cm^{-2}$. Between each addition, the ink was dried for 5 min in air at $T=383$ K to ensure evaporation of the water and the Nafion® solvents, resulting in a so-called "porous" RDE. The working electrode was immersed/emmersed in/from the electrochemical cell at controlled electrode potential: $E=0.40$ V vs. RHE.

In IL-TEM experiments, the electrocatalyst suspension was diluted by a factor of 4 with MQ-grade water (Millipore). A 5-μL aliquot was then deposited over a gold TEM grid and dried in air. The TEM grid was then inserted between two glassy carbon sheets, which served as a mechanical support and current collectors for the electrochemistry experiments. Both plates were held pressed one upon the other by a clamp. The IL-TEM grid was immersed in the electrochemical cell at controlled electrode potential: $E=0.40$ V vs. RHE.

Electrochemical Characterization and Potentiostatic Measurements

Ten cyclic voltammograms were first recorded at 20 mV s^{-1} between 0.05 and 1.23 V vs. RHE followed by a cyclic voltammogram at 100 mV s^{-1} to obtain the characteristic voltammetric response of 40 wt.% Pt/HSAC. The ECSA of

the fresh Pt/HSAC electrocatalyst was then measured using the coulometry of a CO_{ad} stripping voltammogram performed at 100 mV s^{-1}. The CO saturation coverage was established by bubbling CO for 6 min and purging the solution with Ar for 45 min, while keeping the electrode potential at $E=0.10$ V vs. RHE. It was assumed that the electrooxidation of an adsorbed CO monolayer requires 420 μC per cm^2. After the characterization, the electrode was then emmersed at controlled electrode potential $E=0.40$ V vs. RHE and then transferred to the degradation cell with the electrode surface protected by a drop of electrolyte (the overall procedure takes less than a minute). The long-term accelerated stress test performed in this study consisted in potentiostatic measurements at 1.0 V for 96 h. The change in ECSA was monitored with CO_{ad} stripping voltammograms performed at the beginning and at the end of the test, at 0 and 96 h in the characterization cell.

High-Resolution Transmission Electron Microscopy Imaging

The Pt/HSAC nanoparticles were deposited onto a gold grid (300 mesh, Lacey Carbon; Agar Sc. UK), and examined with a JEOL 2010 TEM operated at 200 kV with a point to point resolution of 0.19 nm. Five randomly selected carbon particles located at different places of the TEM grid were imaged at low (80 k) and high (150 k) magnification. After the electrochemical experiments, the TEM grid was rinsed with MQ-grade water, dried in air, and transferred back for TEM analyses in exactly the same position (identical-location TEM) [9, 12, 27–29]. The IL-TEM images were used to build the particle size distribution of the electrocatalysts before/after degradation test. From these observations, the number-averaged mean-particle size:

$$\overline{d}_N = \frac{\sum_{i=1}^{n} n_i d_i}{\sum_{i=1}^{n} n_i} \quad (1)$$

and the surface-averaged mean particle size:

$$\overline{d}_S = \frac{\sum_{i=1}^{n} n_i d_i^3}{\sum_{i=1}^{n} n_i d_i^2} \quad (2)$$

were determined by eye-counting over ca. 400 particles (n_i stands for the number of particles having a diameter d_i). Only "isolated" particles (that is non-agglomerated, single grain spherical particles) were counted to build the particle size distribution. Any other Pt nanoparticle whatever its shape or its structure (a single crystallite or a combination of individual nanocrystallites) was considered an "agglomerated" Pt nanoparticle.

Results and Discussion

Accelerated Stress Tests, Characterization Protocols, and ECSA Changes

The benchmark accelerated stress test used in this study is a potential hold at $E=1.0$ V vs. RHE for 96 h in deaerated electrolyte. Five cyclic voltammograms at 100 mV s^{-1}, one cyclic voltammogram at 20 mV s^{-1}, and one CO_{ad} stripping voltammogram were recorded at the beginning and at the end of the test to monitor the changes in Pt surface reactivity and ECSA. Such experimental conditions are referred to as "AST 0" in what follows (Table 1). The effect of intermediate characterizations, such as cyclic voltammograms or CO_{ad} stripping voltammograms, was investigated by adding different intermediate characterization protocols to the benchmark AST:

- AST 1. In this aging test, five cyclic voltammograms at 100 mV s^{-1}, one cyclic voltammogram at 20 mV s^{-1}, and one CO_{ad} stripping voltammogram were additionally performed after 6, 24, 48, and 72 h to monitor the variations of ECSA over time.
- AST 2. In this aging test, five cyclic voltammograms at 100 mV s^{-1} and one cyclic voltammogram at 20 mV s^{-1} were additionally performed after 6, 24, 48, and 72 h.
- AST 3. In this aging test, one CO_{ad} stripping experiment was additionally performed after 6, 24, 48, and 72 h to monitor the change of ECSA over time.
- AST 4. In this aging test, five cyclic voltammograms at 100 mV s^{-1}, one cyclic voltammogram at 20 mV s^{-1}, and one "pseudo" CO_{ad} stripping voltammogram were performed to monitor the changes in surface reactivity and ECSA. A "pseudo" CO_{ad} stripping experiment consisted of all the steps involved in a normal CO_{ad} stripping but uses Ar instead of CO. Two real CO_{ad} stripping experiments (that is with CO) were performed to monitor the changes in ECSA after polarization at $E=1.0$ V vs. RHE for 96 h in deaerated electrolyte.

Figure 1 and Table 2 show the ECSA changes recorded as a function of the polarization time at $E=1.0$ V vs. RHE for the different aging tests. It is obvious that intermediate characterizations are the major contributor to the decrease of the electrochemically active surface area. Indeed, while the benchmark aging test (96 h at $E=1.0$ V vs. RHE) displays only 5 % ECSA loss (AST 0), the same aging test with the full set of intermediate characterizations features 18 % of ECSA loss (AST 1). It is also clear from Fig. 1 that when only a part of the full characterization protocol is realized (i.e., potential cycling or CO_{ad} stripping), ECSA losses are kept at intermediate values. The most degrading characterization protocol in terms of ECSA losses can be ranked as:

Table 1 Description of the ASTs used in this study

AST	0	1	2	3	4
96 h potential hold at E=1.0 V *vs*. RHE	Yes	Yes	Yes	Yes	Yes
Beginning/end characterizations	Yes	Yes	Yes	Yes	Yes
Type of intermediate characterizations	0	CVs+CO_{ad} stripping voltammograms	CVs	CO_{ad} stripping voltammograms	CVs+"pseudo" CO_{ad} stripping voltammograms

Intermediate CVs (AST 2)<intermediate CVS+"pseudo" CO_{ad} stripping (AST 4)<intermediate CO_{ad} stripping (AST 3)~intermediate CVs+intermediate CO_{ad} stripping (AST 1)

This order suggests that excursions or extended polarization at reducing potentials, such as that performed during the adsorption of a CO monolayer, accelerate the ECSA losses. These results can be understood in view of the breakdown of the passivation layer formed on the Pt/HSAC electrocatalyst during the polarization at E=1.0 V vs. RHE. Indeed, it is well documented that a passivating oxide layer forms on the Pt surface at electrode potential above 1.0 V [30–32]. The reduction of this oxide layer in the negative going-potential scan is accompanied by the dissolution of platinum nanoparticles [30, 33, 34], the quantity of Pt^{z+} ions released in solution increasing with an increase in the duration of a potential cycle [24]. Similarly, extended polarization at high electrode potential causes formation of stable carbon surface oxides (CO_{surf}), but potential excursion below 0.65 V vs. RHE renews the carbon surface and intensifies the carbon corrosion rate [19].

Summing up, these results evidence an intensification of the ECSA changes with the type and the number of intermediate characterizations used to monitor ECSA variations during ASTs. Therefore, a proper evaluation of the ECSA changes requires minimal perturbation of the system, and ideally accurate measurements of the ECSA losses over time would require individual electrodes (for example, in the benchmark AST considered here, five electrodes would then be used: the first one being aged for 6 h, the second for 24 h, and so on until 96 h). This is an important aspect that has to be kept in mind when studying the degradation of PEMFC electrode materials.

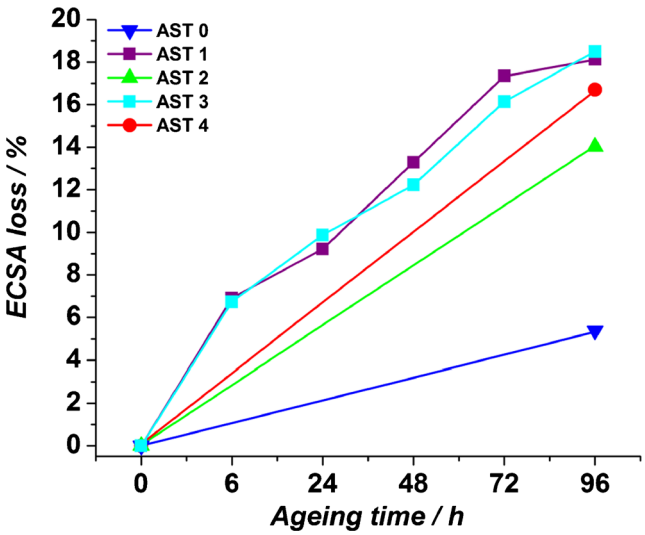

Fig. 1 Evolution of the ECSA for different intermediate characterization protocols. The ECSA was estimated from the CO_{ad} stripping coulometry. Electrolyte: 0.1 M H_2SO_4; v=0.100 V s^{-1}; T=330 K

Electrochemical Characterizations

Further evidences that intermediate characterizations affect the surface chemistry of the Pt/HSAC electrocatalyst are provided by the cyclic voltammograms recorded after the 96-h polarization for the different aging tests. Figure 2 shows the cyclic voltammograms measured before/after the ASTs for different characterization protocols. Note that all the electrodes present similar H_{upd} features (under-potential adsorption/desorption of protons onto/from Pt nanoparticles) and comparable ECSA values (Table 2) indicating that the samples are comparable at the initial stage. However, a decrease of the H_{upd} charge density is noticed for AST 0. Such feature may indicate contamination of the liquid electrolyte of the "degradation cell." However, surface contamination appears very unlikely because (1) all the glassware used in this study was carefully cleaned before its use in Caro acid; (2) during the transfer between the degradation and the characterization cells, the surface of the working electrode was protected by a drop of electrolyte and the transfer procedure takes less than a minute; and (3) this decrease in charge

Table 2 Evolution of the ECSA for the different ASTs used in this study

Accelerated stress test	Fresh ECSA (cm^2)	Aged ECSA (cm^2)	ECSA loss in %
0	8.74	8.27	5.4
1	9.11	7.46	18.1
2	9.27	7.96	14.1
3	9.55	7.81	18.2
4	9.52	7.93	16.7

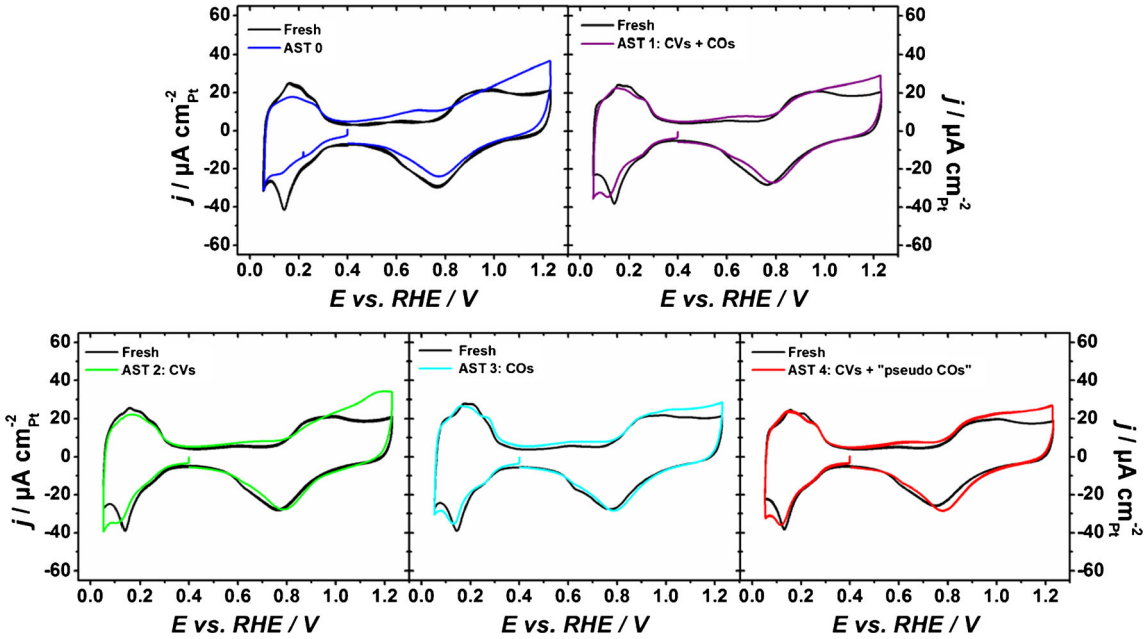

Fig. 2 Cyclic voltammograms measured after the ASTs for different intermediate characterization protocols. The current is normalized to the real surface area estimated from the CO_{ad} stripping coulometry. Electrolyte: 0.1 M H_2SO_4; v=0.020 V s^{-1}; T=330 K

density is perfectly reproducible. It is believed that such features rather indicate that the Pt surface is strongly oxidized by the 96-h potential step at E=1.0 V vs. RHE. Such potential condition favors strong oxidation of the Pt surface, thereby yielding a decrease of the H_{upd} adsorption. Another possible explanation is a contamination of the Pt catalytic sites by oxygen-containing surface groups (CO_{surf}) produced during the electrochemical corrosion of the HSAC (such as quinone/hydroquinone groups). Previous work evidenced that CO_{surf} species may back-spillover from the carbon support to Pt, where they dehydrogenate into adsorbed CO molecules [18]. In any case, our results indicate that integration of the H_{upd} charge is inappropriate for the measurement of the real surface area of the Pt/HSAC electrocatalysts during ASTs.

There is also clear evidence that the charge contained under the quinone–hydroquinone redox couple [35] ($0.5<E<0.8$ V) increases during the 96-h polarization at E=1.0 V vs. RHE, in agreement with what was observed by Kinoshita et al. in phosphoric acid at higher temperature [36]. This trend is particularly marked for the test where no intermediate CV or CO_{ad} stripping voltammogram is performed (AST 0), which suggests that cyclic voltammogramms favor the electrooxidation of CO_{surf} groups in CO_2.

Structural Modifications of the Pt/HSAC Electrocatalysts Followed by IL-TEM

We now focus our attention on the morphological changes of the Pt/HSAC nanoparticles with the help of representative identical location transmission electron microscopy images recorded after the different ASTs mentioned in "Accelerated Stress Tests, Characterization Protocols and ECSA Changes". The comparison between AST 0 and AST 1 allowed quantifying the effect of intermediate characterizations. The AST 3 was used to explore the influence of CO_{ad} stripping voltammograms, and the AST 4 investigated whether this effect is due to the electrochemically reducing potential or to the CO atmosphere.

Recently, a possible limitation of the IL-TEM technique at elevated temperatures has been already discussed in the literature: Schlögl et al. [37] evidenced that, at temperature close to 330 K, the dissolution of the gold TEM grid initiates at potentials higher than 1.3 V vs. RHE, thereby eventually promoting the redeposition of Au^{3+} ions onto Pt/HSAC nanoparticles during excursions at the negative potential limit. Since this upper potential limit of 1.3 V vs. RHE was never exceeded during our ASTs, this phenomenon is very unlikely to have occurred.

Effect of the Number of Intermediate Characterizations

Figures 3 and 4 display IL-TEM micrographs recorded before/after AST 0 and AST 1, respectively. In both ASTs, well-known degradation mechanisms appear: (1) the migration of Pt nanocrystallites, resulting in an increase of the degree of agglomeration (white rectangles), (2) the electrochemical Ostwald ripening, which is preferential dissolution of the smallest Pt nanocrystallites over time (production of Pt^{z+} ions) and the increase of the mean particle size due to redeposition of these ions (green circles), and (3) the thinning/shrinking/

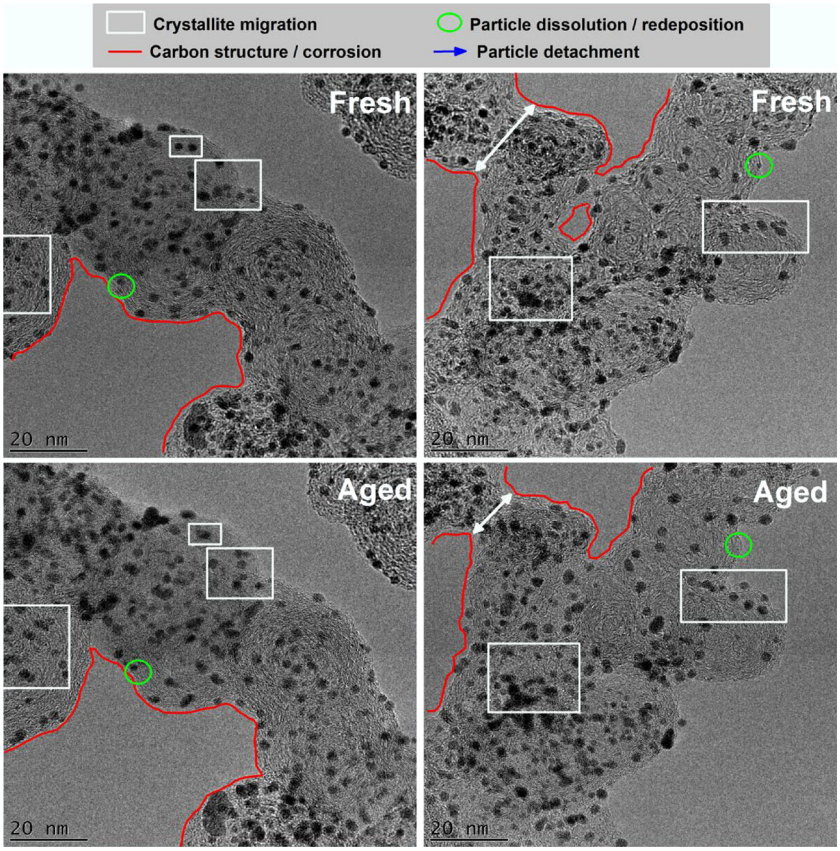

Fig. 3 IL-TEM images of the Pt/HSAC electrocatalyst after AST 0 (96-h polarization at $E=1.0$ V vs. RHE and $T=330$ K in 0.1 M H_2SO_4)

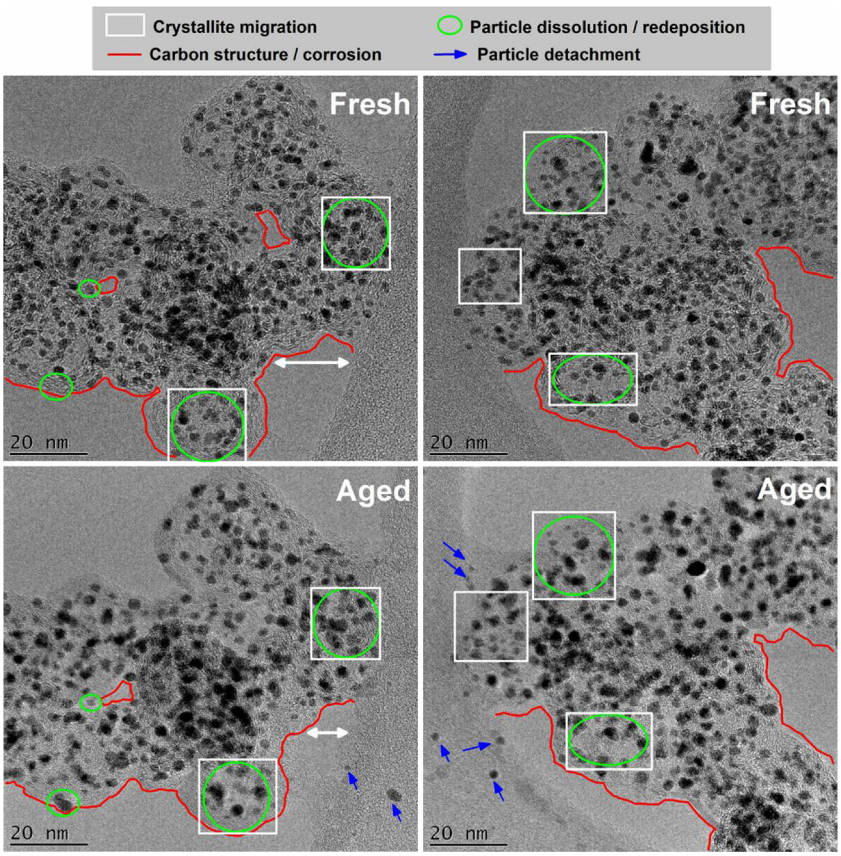

Fig. 4 IL-TEM images of the Pt/HSAC electrocatalyst after AST 1 (96 h-polarization at $E=1.0$ V *vs*. RHE and $T=330$ K in 0.1 M H_2SO_4+intermediate characterizations)

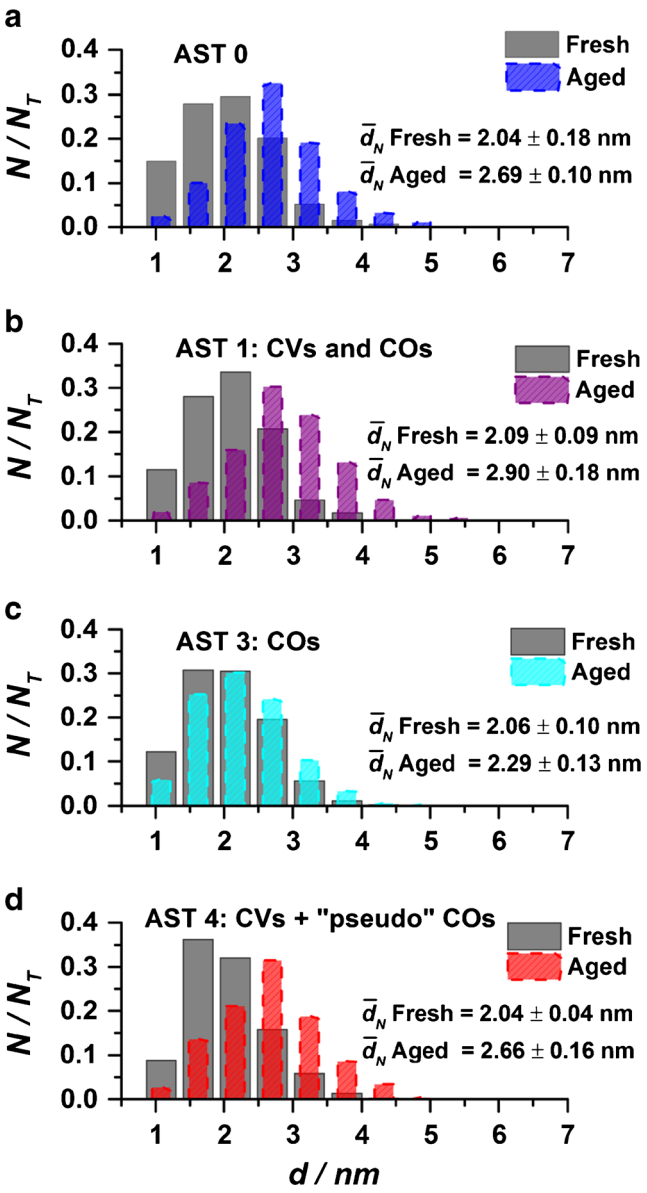

Fig. 5 Particle size distribution and number-averaged diameter ($\overline{d}_N$) for the different ASTs used in this study

collapsing of the carbon particles due to electrochemical corrosion (white arrows) or structural rearrangement of the carbon particles (red line).

However, it is clear from these micrographs that the extent of degradation of the Pt nanoparticles increases with an increase in the number of intermediate characterizations. These observations are quantified in Figs. 5 and 6 where the particle size distributions, the surface-averaged mean particle size, and the density of "isolated" particles are displayed. The Pt nanoparticles increase in size more significantly, and there is a more pronounced decrease in the fraction of small Pt nanocrystallites when intermediate characterizations are implemented in the AST: + 38 % in size for AST 1 vs. + 32 % in size for AST 0. This may be explained by the redeposition of Pt^{z+} ions produced by electrochemical Ostwald ripening during the negative-going potential sweep in cyclic voltammetry experiments.

Furthermore, Fig. 7 illustrates that the changes of the carbon support structure are more severe when intermediate characterizations are included in the AST. For both AST 0 (left-hand side) and AST 1 (right-hand side), the borders of the primary carbon particles are modified, but the brighter contrast of IL-TEM micrographs recorded after AST 1 suggests more pronounced corrosion of the HSAC in this case. Further evidence of this phenomenon is provided in Fig. OR 1 (see Online Resource), which displays Raman spectra measured on the fresh/aged Pt/HSAC electrocatalysts. The greater depreciation of the D-band intensity after AST 1 vs. AST 0 undeniably signs the preferential corrosion of the disorganized domains of the HSAC, in agreement with what was found by Dubau et al. [8, 21]. Considering the above, it is not surprising that Pt nanoparticles detach from the carbon support (blue arrows) during AST 1 (blue arrows in Fig. 4 and Fig. OR 2, see Online Resource) and not in AST 0 (Fig. 3). Proof of this phenomenon is made possible because certain detached Pt nanoparticles are trapped in the Lacey carbon membrane of the TEM grid. It is very likely that Pt nanoparticle detachment may partially account for the 13 % difference in the ECSA loss monitored between AST 0 and AST 1 in RDE configuration. Finally, since the Raman spectra are normalized to the intensity of the G-band, it is difficult to judge if the content in graphitic domains is also impacted by the AST (only the relative ratio of the intensity of the D to the G-band can be visualized).

Effect of the Nature of the Intermediate Characterization

We now discuss the effect of the nature of the intermediate characterizations (cyclic and CO_{ad} stripping voltammograms) used during ASTs. For that purpose, AST 1 that includes four intermediate CVs and 4 CO_{ad} intermediate stripping voltammograms, AST 3 that includes four CO_{ad} intermediate stripping voltammograms, and AST 4 that includes four intermediate CVs and four "pseudo" CO_{ad} stripping voltammograms are compared.

Figure 8 shows the IL-TEM images recorded before/after AST 3. In these experimental conditions, crystallite migration and particle agglomeration appear to be the predominant degradation mechanisms (see inset). Indeed, the mean diameter of the isolated Pt nanoparticles is only slightly altered ($\overline{d}_N$ aged=2.29 nm vs. $\overline{d}_N$ fresh=2.06 nm in Fig. 5) and the population of small Pt nanoparticles (between 1 and 1.5 nm) is preserved (Fig. 6). As proposed in our former study [9], this can be explained by considering that CO molecules partially reduce the CO_{surf} species present on the carbon support, thereby facilitating their movement. A striking result is the

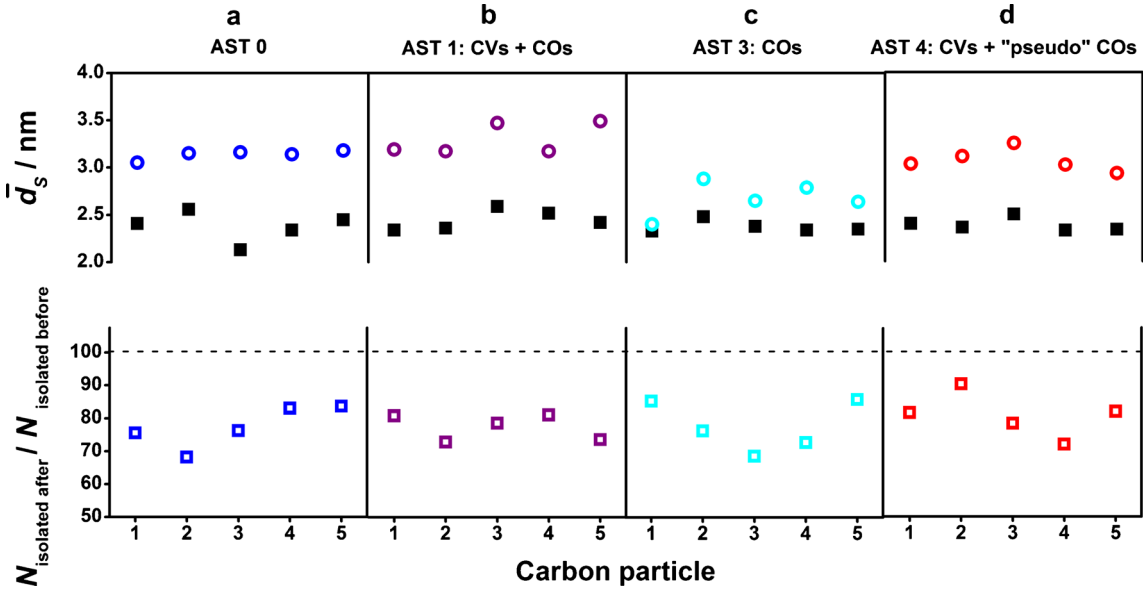

Fig. 6 Surface averaged mean particle size ($\bar{d}_S$) and density of isolated (non-agglomerated and spherical) Pt nanoparticles before (*filled symbols*) and after (*open symbols*) different ASTs

absence of Pt nanocrystallite growth in these AST conditions, which suggests that CO molecules minor the dissolution of Pt into the electrolyte and/or the redeposition of Pt^{z+} ions onto larger crystallites. However, in the latter scenario, a decrease in the mean Pt/HSAC crystallite growth should have been observed.

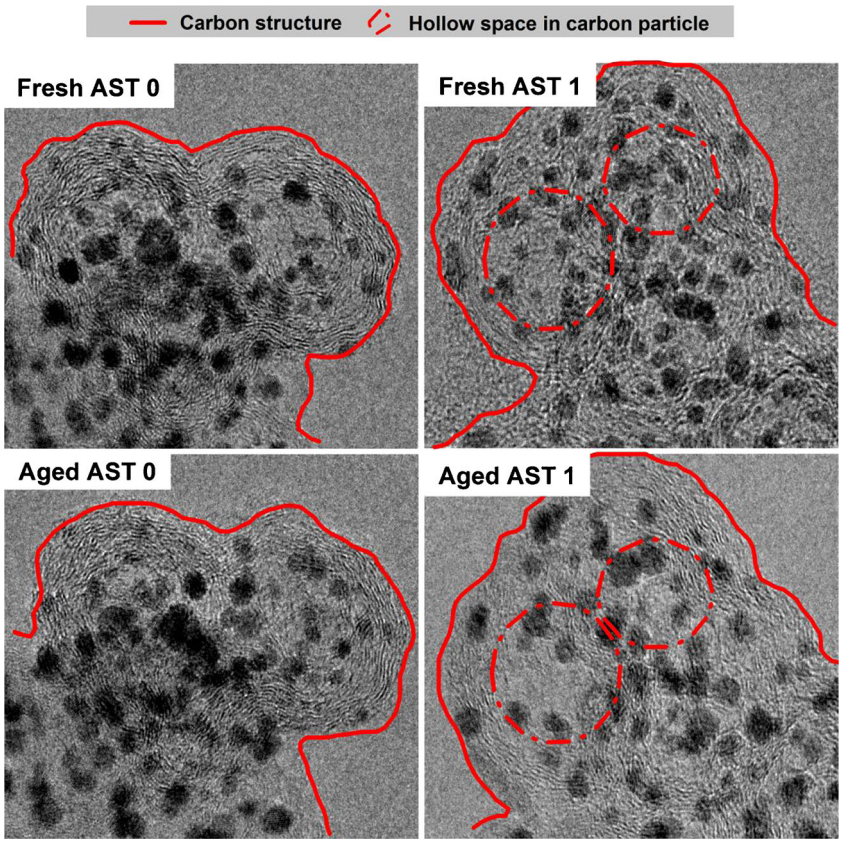

Fig. 7 IL-TEM images of the Pt/HSAC electrocatalyst after AST 0 (96-h polarization at E=1.0 V vs. RHE and T=330 K in 0.1 M H_2SO_4) and AST 1 (96-h polarization at E=1.0 V vs. RHE and T=330 K in 0.1 M H_2SO_4+ intermediate characterizations)

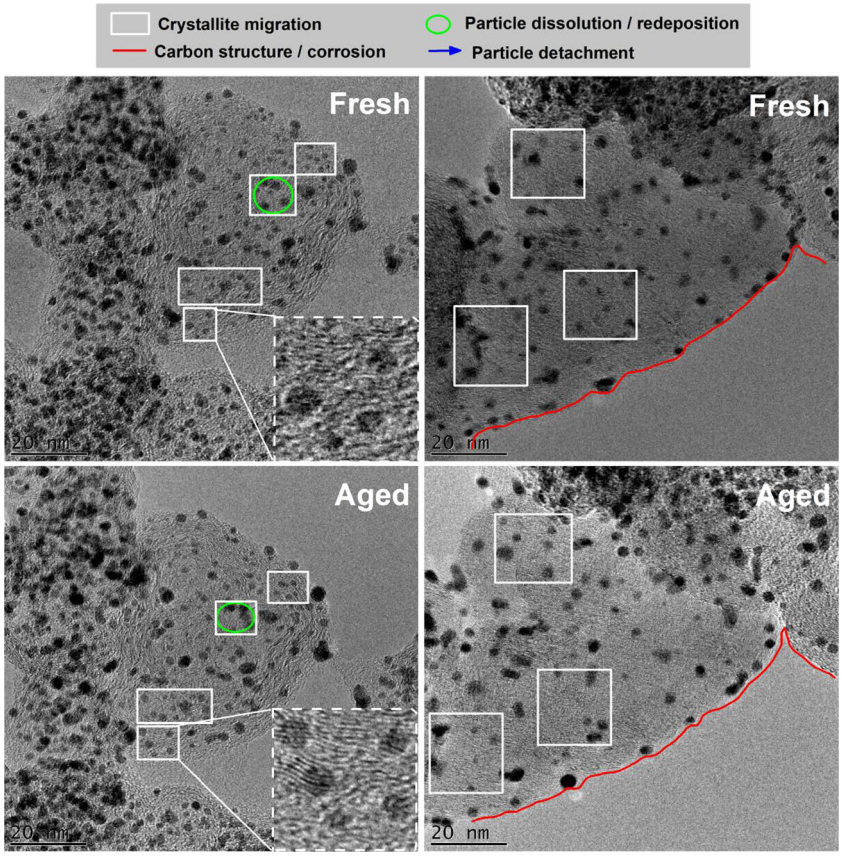

Fig. 8 IL-TEM images of the Pt/HSAC electrocatalyst after AST 3 (96-h polarization at $E=1.0$ V vs. RHE and $T=330$ K in 0.1 M H_2SO_4+CO_{ad} stripping voltammograms)

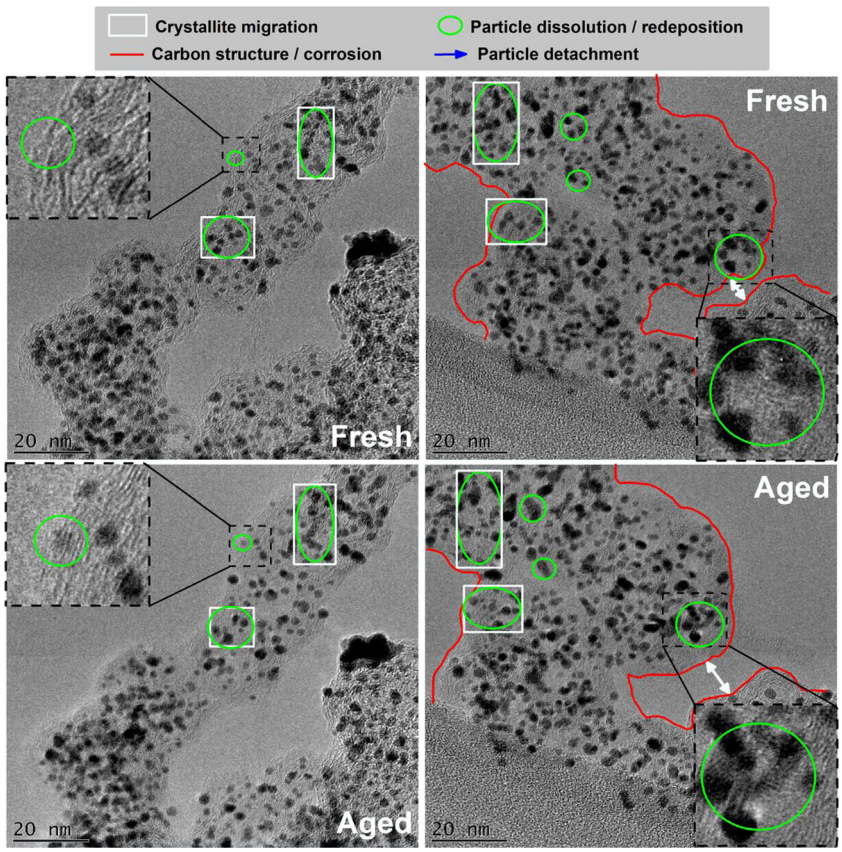

Fig. 9 IL-TEM images of the Pt/HSAC electrocatalyst after AST 4 (96-h polarization at $E=1.0$ V vs. RHE and $T=330$ K in 0.1 M H_2SO_4+CVs+"pseudo" CO_{ad} stripping voltammograms)

Further evidence of the influence of CO molecules can also be seen in Fig. 9, which presents representative IL-TEM images for AST 4. This AST is essentially similar to AST 1, except that Ar was bubbled in solution during the CO_{ad} stripping experiments ("pseudo" CO_{ad} stripping voltammograms). In this case, in addition to particle migration/agglomeration, the dissolution/redeposition of Pt nanocrystallites is evidenced by the appearance of Pt nanoparticles that were not present in the fresh state or the formation of flat rafts between individual Pt nanocrystallites (Fig. 9, inset). Moreover, similar variations of the density of isolated Pt nanoparticles and of the mean Pt nanoparticle size were observed during AST 4 and AST 1 (Figs. 5 and 6). This confirms that CO molecules minor the dissolution of Pt nanoparticles into Pt^{z+} ions, in agreement with our former results [9].

Conclusion

In this study, we showed that the intermediate characterizations performed during accelerated stress tests intensify the ECSA losses. In the present experimental protocol, potentiostatic hold at $E = 1.0$ V vs. RHE during 96 h, intermediate characterizations (cyclic voltammetry and CO_{ad} stripping experiments) cause the major part of ECSA losses. These characterizations are required to access the ECSA changes during the AST but actually level off the "real" degradation rate of the Pt/HSAC electrocatalysts (similar ECSA losses, ~18 %, were found for AST 1 whatever the value of the electrode potential in the range $0.40 < E < 1.20$ V vs. RHE, see Fig. OR 3 in Online Resource). By using IL-TEM and electrochemical techniques, the structural modifications of the Pt/HSAC nanoparticles could be monitored. The main conclusions are the following: (1) intermediate characterizations exacerbate characteristic degradation mechanisms of Pt/HSAC nanoparticles: Pt nanocrystallite migration/agglomeration, corrosion of the carbon support, and greatly promote the redeposition of Pt^{z+} ions produced by electrochemical Ostwald ripening (more pronounced Pt particle growth), (2) intermediate characterization modify the chemistry of the Pt nanocrystallites and of the high surface area carbon support during potentiostatic ASTs, and (3) adsorbed CO molecules minor the dissolution of Pt^{z+} ions. Consequently, neither CVs (more facile redeposition of Pt^{z+} ions) nor CO_{ad} stripping voltammograms proved to be adapted to proper and safe monitoring of the ECSA variations during potentiostatic ASTs. Our study highlights that the number and the nature of intermediate characterizations should be controlled when designing new accelerated stress tests. Ideally, individual electrodes should be used to get an accurate evaluation of the ECSA variations over time during ASTs.

Acknowledgments The authors acknowledge financial support by Oseo-AII through the H2E project and Alexandre Crisci of the Consortium des Moyens Technologiques Communs (CMTC) of Grenoble INP for the Raman spectroscopy measurements.

References

1. H.A. Gasteiger, S.S. Kocha, B. Sompalli, F.T. Wagner, Appl. Catal., B **56**, 9 (2005)
2. R. Borup, J. Meyers, B. Pivovar, Y.S. Kim, R. Mukundan, N. Garland, D. Myers, M. Wilson, F. Garzon, D. Wood, P. Zelenay, K. More, K. Stroh, T. Zawodzinski, J. Boncella, J.E. McGrath, M. Inaba, K. Miyatake, M. Hori, K. Ota, Z. Ogumi, S. Miyata, A. Nishikata, Z. Siroma, Y. Uchimoto, K. Yasuda, K.-I. Kimijima, N. Iwashita, Chem. Rev. **107**, 3904 (2007)
3. M.K. Debe, Nature **486**, 43 (2012)
4. L. Dubau, F. Maillard, M. Chatenet, J. André, E. Rossinot, Electrochim. Acta **56**, 776 (2010)
5. L. Dubau, F. Maillard, M. Chatenet, L. Guetaz, J. André, E. Rossinot, J. Electrochem. Soc. **157**, B1887 (2010)
6. E. Billy, F. Maillard, A. Morin, L. Guetaz, F. Emieux, C. Thurier, P. Doppelt, S. Donet, S. Mailley, J. Power Sources **195**, 2737 (2010)
7. L. Dubau, J. Durst, F. Maillard, L. Guétaz, M. Chatenet, J. André, E. Rossinot, Electrochim. Acta **56**, 10658 (2011)
8. L. Dubau, M. Lopez-Haro, L. Castanheira, J. Durst, M. Chatenet, P. Bayle-Guillemaud, L. Guétaz, N. Caqué, E. Rossinot, F. Maillard, Appl. Catal., B **142–143**, 801 (2013)
9. L. Dubau, L. Castanheira, G. Berthomé, F. Maillard, Electrochim. Acta **110**, 273 (2013)
10. Z. Zhao, L. Dubau, F. Maillard, J. Power Sources **217**, 449 (2012)
11. B. Vion-Dury, M. Chatenet, L. Guétaz, F. Maillard, ECS Trans. **41**, 697 (2011)
12. J.C. Meier, I. Katsounaros, C. Galeano, H.J. Bongard, A.A. Topalov, A. Kostka, A. Karschin, F. Schüth, K.J.J. Mayrhofer, Energy Environ. Sci. **5**, 9319 (2012)
13. K. Yasuda, A. Taniguchi, T. Akita, T. Ioroi, Z. Siroma, Phys. Chem. Chem. Phys. **8**, 746 (2006)
14. E. Guilminot, A. Corcella, F. Charlot, F. Maillard, M. Chatenet, J. Electrochem. Soc. **154**, B96 (2007)
15. K.H. Kangasniemi, D.A. Condit, T.D. Jarvi, J. Electrochem. Soc. **151**, E125 (2004)
16. S. Maass, F. Finsterwalder, G. Frank, R. Hartmann, C. Merten, J. Power Sources **176**, 444 (2008)
17. B. Avasarala, R. Moore, P. Haldar, Electrochim. Acta **55**, 4765 (2010)
18. F. Maillard, A. Bonnefont, F. Micoud, Electrochem. Commun. **13**, 1109 (2011)
19. N. Linse, L. Gubler, G.G. Scherer, A. Wokaun, Electrochim. Acta **56**, 7541 (2011)
20. A. Zana, J. Speder, M. Roefzaad, L. Altmann, M. Bäumer, M. Arenz, J. Electrochem. Soc. **160**, F608 (2013)
21. Z. Zhao, L. Castanheira, L. Dubau, G. Berthomé, A. Crisci, F. Maillard, J. Power Sources **230**, 236 (2013)
22. U. S. C. f. A. R. LLC (2011), www.uscar.org/guest/view_team.php?teams_id=17. Accessed 17 July 2013
23. A. Ohma, K. Shinohara, A. Iiyama, T. Yoshida, A. Daimaru, ECS Trans. **41**, 775 (2011)
24. A.A. Topalov, I. Katsounaros, M. Auinger, S. Cherevko, J.C. Meier, S.O. Klemm, K.J.J. Mayrhofer, Angew. Chem., Int. Ed. **51**, 12613 (2012)
25. K. Kinoshita, J.T. Lundquist, J. Bett, Electr. Chem. Interfac Electrochem. **48**, 157 (1973)

26. C.C. Herrmann, G.G. Perrault, A.A. Pilla, Anal. Chem. **40**, 1173 (1968)
27. K.J.J. Mayrhofer, S.J. Ashton, J.C. Meier, G.K.H. Wiberg, M. Hanzlik, M. Arenz, J. Power Sources **185**, 734 (2008)
28. K.J.J. Mayrhofer, J.C. Meier, S.J. Ashton, G.K.H. Wiberg, F. Kraus, M. Hanzlik, M. Arenz, Electrochem. Commun. **10**, 1144 (2008)
29. F.J. Perez-Alonso, C.F. Elkjaer, S.S. Shim, B.L. Abrams, I.E.L. Stephens, I. Chorkendorff, J. Power Sources **196**, 6085 (2011)
30. V.I. Birss, M. Chang, J. Segal, J. Electroanal. Chem. **355**, 181 (1993)
31. Z. Nagy, H. You, Electrochim. Acta **47**, 3037 (2002)
32. X.P. Wang, R. Kumar, D.J. Myers, Electrochem. Solid State Lett. **9**, A225 (2006)
33. S.G. Rinaldo, W. Lee, J. Stumper, M. Eikerling, Electrochem. Solid State Lett. **14**, B47 (2011)
34. D.C. Johnson, D.T. Napp, S. Bruckenstein, Electrochim. Acta **15**, 1493 (1970)
35. K. Kinoshita, *Carbon: electrochemical and physicochemical properties* (Wiley, New York, 1988)
36. K. Kinoshita, J. Bett, Carbon **11**, 237 (1973)
37. K. Schlögl, K.J.J. Mayrhofer, M. Hanzlik, M. Arenz, J. Electroanal. Chem. **662**, 355 (2011)